Eurasian Chemico-Technological Journal 17 (2015) 3-15

Graphene Based Biomedical Composite Coatings Produced by Electrophoretic Deposition on Titanium

V. Mišković-Stanković[1]*, A. Janković[1], S. Eraković[1] and K. Yop Rhee[2]

[1]Faculty of Technology and Metallurgy, University of Belgrade,
Karnegijeva 4, 11000 Belgrade, Serbia
[2]Department of Mechanical Engineering, Kyung Hee University,
Yongin, 449-701 Korea

Abstract

The biocomposite hydroxyapatite/graphene (HAP/Gr) and silver/hydroxyapatite/graphene (Ag/HAP/Gr) coatings were electrodeposited on titanium substrate using the electrophoretic deposition (EPD) technique to produce bioactive coating with improved mechanical characteristics and corrosion stability in simulated body fluid (SBF). The electrodeposited coatings were characterized by scanning electron microscopy, Raman spectroscopy, X-ray diffraction, Fourier transform infrared spectroscopy, thermogravimetric analysis, X-ray photoelectron analysis, nanoindentation test and electrochemical impedance spectroscopy. Both HAP/Gr and Ag/HAP/Gr coatings exhibited reduced surface cracks, better mechanical resistance, enhanced thermal and corrosion stability, as well as bioactivity No antibacterial activity against *Staphylococcus aureus* and *Escherichia coli* was verified in the case of HAP/Gr coating, while Ag/HAP/Gr coating exhibited antibacterial activity indicating the high potential for biomedical applications. Both coatings were classified as non-cytotoxic against healthy peripheral blood mononuclear cells (PBMC).

1. Introduction

Today's materials science bright stars: zero-dimensional (0D) fullerenes, 1D carbon nanotubes (CNTs) and two-dimensional (2D) graphene sheets (single layer sp^2-hybridized carbon atoms packed in a honeycomb manner) have been only recently discovered [1, 2]. However, due to extraordinary electrical, thermal, excellent mechanical properties and high specific surface area that this new material possesses, especially favored application of graphene (Gr) is reinforcement for the future composite materials [1–3]. Most recent research reports reveal that e.g. graphene nanosheets (GNs), comprised layers of Gr (thickness up to 100 nm) [4] are not difficult to produce and could be engaged with success as nanofillers to polymers [5], metals [6] and ceramics [3, 7]. Thus formed composites retained exceptional mechanical properties [3].

Implant materials are in direct contact with fragile surrounding that human body represents. However, that sensitive environment due to its salt composition and pH value, acts as a corrosive agent to metallic devices. Therefore, the idea of applying a versatile coating that would represent a barrier for metabolic influences became very interesting, especially in a context that such material could even bring a much needed additional bioactivity. Synthetic hydroxyapatite ($Ca_{10}(PO_4)_2(OH)_2$, HAP), chemically similar to bone mineral has been used in order to elevate biocompatibility of metallic implants, e.g. Ti or alloys, since they lose their functionality due to degradation from wear, disease, injury [8, 9] or metallic ions leaching into biological surroundings. HAP is bioactive, biocompatible and is able to initiate osteogenesis, but its major weakness is its brittleness, poor mechanical properties, as low fracture toughness (0.8–1.2 MP), low flexural strength (<140 MPa) and wear resistance [10]. Therefore, the idea of improving mechanical performance of hydroxyapatite by combining it with reinforcements becomes a necessity.

---

* Corresponding author. E-mail: vesna@tmf.bg.ac.rs

Special interest in Gr or its derivates for reinforcement of HAP-based biocomposites comes mainly from mechanical reinforcement, but also to recent reports of favorable biological performances of Gr [8]. Recent literature focuses on obtaining HAP composites by utilizing various physico-chemical methods, e.g. reported *in situ* synthesis method [11, 12], spark plasma sintering (SPS) technique [13], biomimetic mineralization process [14, 15], chemical vapor deposition [16] and electrospinning method [17].

The brittleness of thus formed biocomposites is defeated by decreasing crack deflection within the material itself. However, it is proven to be more effective in the case of sheet-like reinforcement (GNSs) than for tubular-like reinforcement (CNTs) [18]. CNTs also pose a potential threat due to their cytotoxicity since they are synthesized in the presence of metallic catalyst particles [19, 20]. Amongst many advantages, qualities of Gr and graphene-based composites include low toxicity toward human osteoblasts [21], antibacterial properties [22] and possible apatite mineralization [23].

Implant biomaterials, as previously postulated, inside the human body challenge the host immune response. Additional threat possesses the presence of bacteria on all affected areas (surgical area and/or implantation site) therefore influencing the clinical dose of antibiotics needed to protect against infection. Antimicrobial properties of silver ions have been known for centuries with the renewed special interest due to microbial antibiotic resistance on biomaterials and medical devices [24]. Especially advantageous properties of the active Ag ion is low toxicity toward human cells and a long lasting biocidal effect due to high thermal stability and low volatility [25].

To assemble bioactive ceramic or composite coatings on various metal surfaces, electrophoretic deposition (EPD) emerged as preferential processing technique. The technique stems from electrochemical properties of colloidal solutions from which the depositions are done. EPD has many advantages e.g. high deposition rate, good control of deposition parameters that affect coating thickness, crystallinity as well as possible deposition on substrates of complex shape; all favorable for the purpose of orthopedic applications with improved, bioactivity, biocompatibility and corrosion resistance [26-32].

The necessary condition that provides successful electrophoretic deposition is a stable suspension/sol, in which the particles have high zeta potential, while the ionic conductivity of the suspension is kept at low value. Factors influencing the EPD process are electrical conditions (voltage and time) and parameters related to suspension (particle charging, solid loading, dispersants, suspension viscosity, particle size distribution). According to the proposed mechanism [33], the deposition process occurs in several steps. Charged particles attract oppositely charged ions (e.g., counterions) around the particles. In the case of cataphoretic deposition positively charged particles migrate toward the cathode. The rate of migration that the particles can achieve, v, depends on applied electric field, E, suspension viscosity, η, particle radius, r, and particle charge, z, and is given by equation:

$$v = z\,E\,/\,6\pi\eta r \tag{1}$$

indicating the linear dependence of migration rate upon applied electric field. Because the particles are close enough to the cathode, attractive forces dominate and coagulation/deposition occurs. In the case of cataphoretic deposition of ceramic coatings on a metal electrode, the primary process is the OH^- ions generation and hydrogen evolution on the cathode by H_2O discharge.

$$2H_2O + 2e^- \rightarrow H_2 + 2OH^- \quad (\text{pH } 7\text{–}14) \tag{2}$$

or

$$2H^+ + 2e^- \rightarrow H_2 \quad (\text{pH } 1\text{–}7) \tag{3}$$

followed by electrocoagulation of the ceramic particles at the cathode surface by neutralization of positively charged groups with electrochemically generated OH^- ions. The deposition of a coating will occur when the hydroxyl ion concentration at the cathode achieves a critical value:

$$R^+ + OH^- \rightarrow \text{film} + H_2O \tag{4}$$

At the same time, the oxygen evolves on the anode:

$$2H_2O \rightarrow 4H^+ + O_2 + 4e^- \tag{5}$$

Evolved hydrogen on the cathode (Eq. (2)) goes out through the coating, leaving the vacancies inside the deposited film and causing its porous structure.

In this study the novel nanoscale composite hydroxyapatite/graphene (HAP/Gr) and silver/hydroxyapatite/graphene (Ag/HAP/Gr) coatings were electrodeposited on Ti using EPD technique, in order to obtain bioactive coatings with favorable corrosion stability in simulated body fluid (SBF) and improved mechanical characteristics. Therefore, our goal was to explore potential of implementing GNs as reinforcement to HAP for load-bearing orthopedic applications.

2. Effect of Graphene on HAP/Gr and Ag/HAP/Gr Coatings

2.1. Electrophoretic Deposition of HAP/Gr and Ag/HAP/Gr Coatings on Titanium Substrate

Nanosized HAP powder was synthesized using a modified chemical precipitation method that required the reaction of calcium oxide (obtained by aerobic calcination of $CaCO_3$ for 5 h at 1000 ºC) and phosphoric acid, according to our previously reported protocol [24, 34]. The final suspension was spray-dried at 120 ± 5 ºC into granulated powder. A nanosized Ag/HAP powder was also prepared utilizing the same modified chemical precipitation protocol except for the addition of silver nitrate [24, 34]. Silver ion concentration was kept at 0.4 ± 0.1 wt.% in the final powder. Ti from Aldrich (foil, thickness 0.25 mm, 99.7% trace metals basis) was used as a substrate for electrophoretic deposition of HAP/Gr and Ag/HAP/Gr coatings. Ti samples were cut in various sizes depending on the intended type of analysis (25 mm × 10 mm for surface analysis, 40 mm × 20 mm for impedance measurements, and 10 mm × 5 mm for cell based assays). Mechanical pretreatment of Ti plates was done according to a previously established protocol [24, 35]. Grit emery paper was used for initial polishing and finalized with 0.3 μm wet alumina. Subsequently, plates were degreased in acetone and ethanol for 15 min each in an ultrasonic bath.

The Gr nanopowder (AO-3), purity 99.2%, was purchased from Graphene Supermarket, USA. The average thickness of the Gr nanoflakes was 12 nm. Approximately 30–50 layers of Gr monolayers were overlapped. Electrophoretic deposition was done from 100 mL of absolute ethanol suspension containing 1 wt.% of nanosized HAP, or 1 wt.% of nanosized Ag/HAP powder (silver content 0.4 ± 0.1 wt.%) and 0.01 wt.% of Gr at pH = 2.00. The prepared HAP/Gr or Ag/HAP/Gr suspension was ultrasonicated for 30 min to maximize homogeneity. During deposition, the suspensions were stirred constantly. A three-electrode cell arrangement was used for cathodic electrodeposition. A pretreated Ti plate served as a working electrode and a substrate for composite coatings deposition. The counter electrodes were two pure platinum panels, placed parallel to the Ti 1.5 cm away, thus assuring uniform coating on both sides of the foil. The composite coatings were deposited using the constant voltage method at 60 V and a deposition time of 2 min at room temperature. Electrodeposited coatings were dried at room temperature [36].

2.2. Characterization methods

The surface morphology of composite coatings, before and after immersion in SBF, was analyzed by field-emission scanning electron microscopy (FE-SEM) using a LEO SUPRA 55, Carl Zeiss, Germany, operated at an acceleration voltage of 200 kV and a TESCAN MIRA 3 XMU. Fourier transform infrared (FT-IR) spectroscopy was carried out using KBr pellets in a Perkin Elmer (spectrum one system) spectrophotometer Standardized scans were performed in the range of 450–4000 cm^{-1}, spectral resolution of 0.5 cm^{-1}. X-ray photoelectron spectroscopy (XPS) measurements were carried out using a K-Alpha System (Thermo electron) equipped with Al Kα X-ray radiation (1486.6 eV) and a micro-focused monochromator. The elemental profile was carried out using Ar-ion sputtering. HR-Raman analysis employed Renishaw in Via Raman spectrophotometer equipped with a 514 nm argon laser, operating at 10% of total power (50 mW). Thermogravimetric and differential thermal (TGA/DTA) analysis was conducted using a TA instrument (TGA Q5000 IR/ SDT Q600) from 30–1000 ºC in nitrogen flow (50 mL/min), heating rate of 20 ºC/ min.

All deposited composite coatings on Ti plates were analyzed to measure the hardness and Young's modulus of the material. A nanoindentation test was conducted on a Hysitron TriboScope nanomechanical system with an in situ imaging mode equipped with a Berkovich indenter at an applied force of 10,000 μN. Loading and unloading rates were kept at 2000 μN/s without holding time. Eight to twelve indentations at different spots of the coating were made for each sample.

Corrosion stability was analyzed based on EIS measurements during prolonged exposure time in SBF at 37 ºC. The working electrode, the coated Ti plate, had a testing surface area of 1 cm^2. The counter electrode was a platinum mesh, and the reference electrode was a saturated calomel electrode (SCE). The impedance data were collected at the open-circuit potential using Reference 600TM Potentiostat/Galvanostat/ZRA (Gamry Instruments, Inc., Warminster, PA, USA) over a wide frequency range (300 kHz–10 mHz) using a 5 mV amplitude of sinusoidal voltage.

2.3. Surface morphology and microstructure analysis

The surface morphology of the as-prepared HAP, Ag/HAP, HAP/Gr and Ag/HAP/Gr composite coatings after air drying at room temperature is shown in Fig. 1. Compared with the surface between graphene-based and their pure coatings, the HAP/Gr (Fig. 1a) and Ag/HAP/Gr (Fig. 1c) composite coatings revealed fewer cracks than their pure forms such as HAP (Fig. 1b) and Ag/HAP (Fig. 1d) coatings, indicating that Gr effectively acts as nano-reinforcement filler and prevents the creation and propagation of cracks by crack bridging as the major toughening mechanism [3]. In order to assess the crack distribution per each sample, Image-J software was employed. Normalized number of cracks per same area (0.1 mm^2) gave about 50% decrease on average in crack number for HAP/Gr (97) compared to pure HAP coating (167). In the case of Ag/HAP/Gr, decrease in crack number (58) was even more pronounced, about 80% compared to the non-graphene containing counterpart Ag/HAP (307). Based on this data it is evident that graphene presence remarkably reduces crack propagation in the material.

The bonding strength between Gr and HAP grains is significantly enhanced due to high specific surface area of graphene nanosheets, thus forming an increased contact area for bonding with matrix.

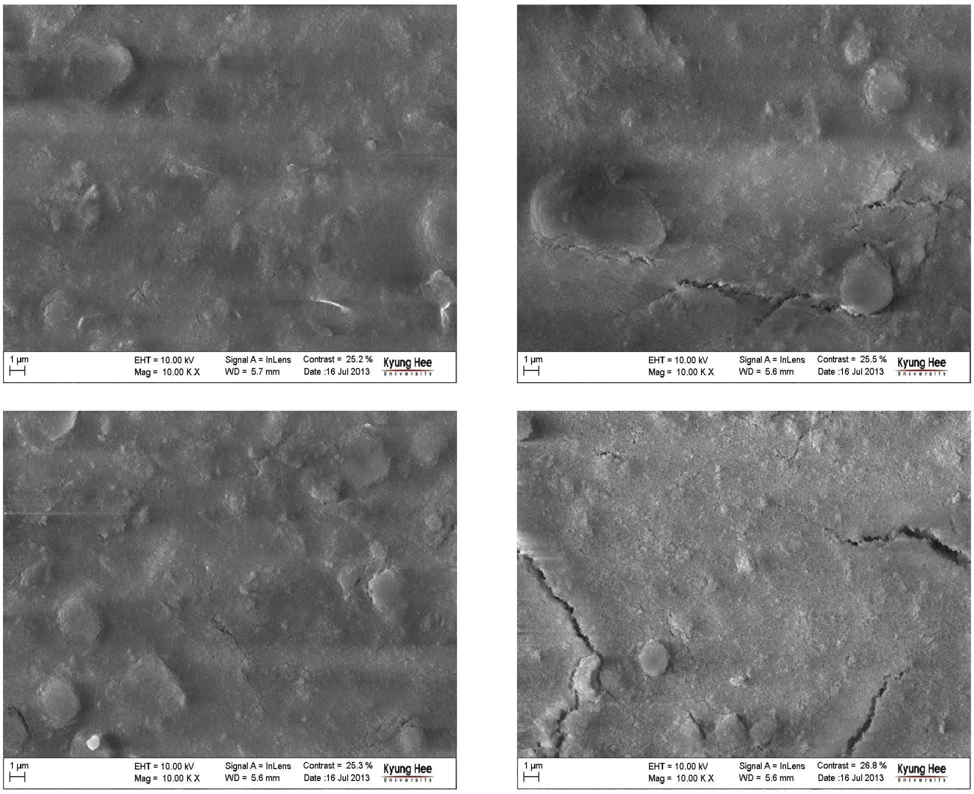

Fig. 1. SEM micrographs of HAP/Gr (a), HAP (b), Ag/HAP/Gr (c) and Ag/HAP (d) coatings, taken under the same magnification (10,000×).

FT-IR spectrum results of HAP/Gr and Ag/HAP/Gr biocomposites verify the efficient transfer by EPD of HAP and Gr as well as the possible bonding within, as it is shown in Fig. 2. In the FT-IR spectra of graphene-based coatings, the three strong bands of the phosphate were all clearly observed in the following range 950–1110 cm^{-1} in the ν_3 and ν_1 mode region (Fig. 2a). The doublet peaks of P-O bend (560 and 601 cm^{-1}) were also well observed in FT-IR spectra (data not shown) [10]. The absorption band at 630 cm^{-1} corresponds to structural OH$^-$ groups in the HAP lattice [37], and the band at 875 cm^{-1} indicates the presence of acidic phosphate group HPO_4^{2-} due to the P-(OH) stretching vibration (data not shown) [10, 37]. In Fig. 2b the absorbance bands in the range of 1500–1400 cm^{-1} correspond to ν_3 asymmetrical stretching vibrations of the CO_3^{2-} ions [39]. The position of the carbonate bands indicates predominately B-type HAP, which is the preferential substitution in human bones due to its excellent bioactivity and osteoinductivity [39]. Very small bands at ~1540 cm^{-1} are assigned to the skeletal vibration of Gr [40, 41] due to sp^2 hybridized C=C vibration stretching, confirming its presence in the composite graphene-based coatings.

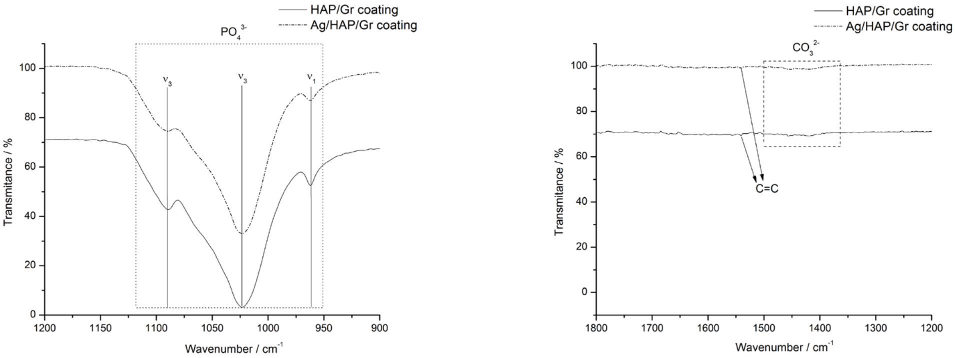

Fig. 2. FT-IR spectra of Ag/HAP/Gr and HAP/Gr coatings, in the wavenumber range 900–1200 cm^{-1} (a) and 1200–1800 cm^{-1} (b).

Table 1

Atomic percentages and Ca/P ratio at sample surface of the Ag/HAP/Gr, Ag/HAP, HAP/Gr and HAP coatings determined by XPS

	Element, %							
Sample	P2p	C1s	Ca2p$_{3/2}$	Ca2p$_{1/2}$	O1s	Ag3d	Ti2p	Ca/P
Ag/HAP/Gr	14.56	12.05	14.97	7.14	50.99	0.15	0.4	1.52
Ag/HAP	16.70	-	16.96	8.08	58.01	0.11	0.14	1.50
HAP/Gr	14.20	11.90	15.16	7.33	51.32	-	0.09	1.58
HAP	16.36	-	16.69	7.86	58.93	-	0.16	1.50

The surface elements of the HAP/Gr and Ag/HAP/Gr composite coatings as well as their non-graphene containing counterparts HAP and Ag/HAP coatings were characterized by XPS and the comparative quantitative analysis of the XPS spectra is presented in Table 1. For the HAP/Gr coating, survey spectrum (Fig. 3) revealed the anticipated presence of Ca2p, P2p and O1s main peak signals, along with an additional peak related to Ti2p. Detailed analysis [36] of Ca2p spectrum reveals a doublet with Ca2p$_{3/2}$ (BE = 347.29 eV) and Ca2p$_{1/2}$ (BE = 350.82eV), and the P2p spectrum reveals a single P2p peak at BE = 133.33 eV, indicating the presence of HAP [42, 43]. The main O1s peak component at BE = 531.27 eV for the HAP/Gr coating is attributed to PO_4^{3-} groups incorporated within apatite lattice [44]. Incorporation of Gr and the formation of the new composite are clearly evidenced by the presence of C1s in the HAP/Gr coating, whereas no trace of carbon is detected in the pure HAP coating. According to the literature, the C1s peak with BE = 285.0 eV is attributed to aromatic hydrocarbons [45], which is in excellent compliance with the single-sheet Gr structure of honeycomb six-membered rings.

Ag/HAP/Gr coating XPS spectra [46] exposed the same surface elements; calcium phosphates (Ca2p doublet, Ca2p$_{3/2}$ (BE = 347.3 eV) and Ca2p$_{1/2}$ (BE = 350.8 eV) and the P2p spectrum with a single P2p peak (BE = 133.3 eV) [41, 42]. The XPS narrow scan spectra of Ag element is present in both Ag/HAP and Ag/HAP/Gr coatings (Table 1). The peak for Ag3d peak (BE = 369.5 eV) agrees well with the literature data [44]. Main peak of O1s at binding energy of 531.3 eV for Ag/HAP/Gr coating is attributed to the presence of PO_4^{3-} groups [43].

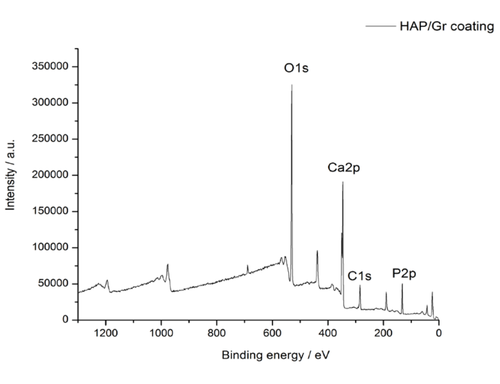

Fig. 3. XPS survey spectra of HAP/Gr coating.

Even though the ideal Ca/P ratio for stoichiometric HAP is known to be 1.67, stable HAP phases have been found to exist over a range of Ca/P ratios from 1.3 to 1.8 [42]. Therefore, our HAP/Gr and Ag/HAP/Gr coatings represent hybrid coatings with a Ca/P ratio of 1.58 and 1.52, respectively, which is greater than that of the pure HAP and Ag/HAP coatings, 1.50 (Table 1), and closer to the stoichiometric value (Ca/P = 1.67) [36, 46].

Raman spectroscopy was utilized to verify the incorporation of graphene in composite HAP/Gr and Ag/HAP/Gr coatings. As depicted in Fig. 4 the Raman spectra reveals a distinct pattern of single-layer Gr and is generally characterized by two main features. The first main feature is the G-peak (the E_{2g} mode of sp^2 carbon atoms), visible at around 1550 cm^{-1}, which arises due to the in-plane vibration of sp^2 carbon atoms [47]. The G-band corresponds to ordered sp^2-bonded carbon atoms. The second pronounced band for both graphene-based composites is the D-peak (the symmetry A_{1g} mode) at 1350 cm^{-1} that represents defects originating from the disordered sp^3-bonded carbon atoms in the Gr edges [48]. The low intensity of both the D and G peaks can be attributed to a very low concentration of Gr [36]. Also observed are 2D band at around 2650 cm^{-1} and the band around 2910 cm^{-1} assigned to D+G band, a state of slightly increased disorder commonly seen in biocomposites.

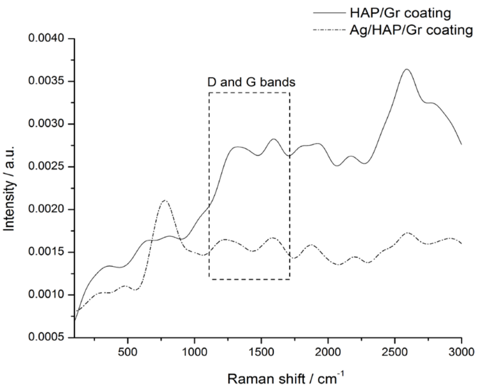

Fig. 4. Raman spectra of the Ag/HAP/Gr and HAP/Gr coatings with D and G bands.

The key feature was to explore thermal stability of EPD-assembled HAP/Gr and Ag/HAP/Gr coatings that were subjected to thermogravimetric analysis in order to observe the characteristic of physical and chemical changes. The thermogravimetric (TG) curves (Fig. 5, for HAP/Gr coating) revealed the weight loss of the HAP/Gr and Ag/HAP/Gr coatings in the observed temperature range between 25 and 1000 ºC. The total weight loss for the HAP/Gr and Ag/HAP/Gr coatings in chosen temperature range was 5.28 and 7.12 wt.%, respectively, confirming the greater thermal stability of graphene-based coating compared to their pure counterparts as reference, which lost 7.16 (HAP) and 7.90 wt.% (Ag/HAP), respectively [36, 46]. The thermal stability of graphene-based composites was substantially improved as a consequence of bonding mechanism between graphene sheets and hydrohyapatite lattice.

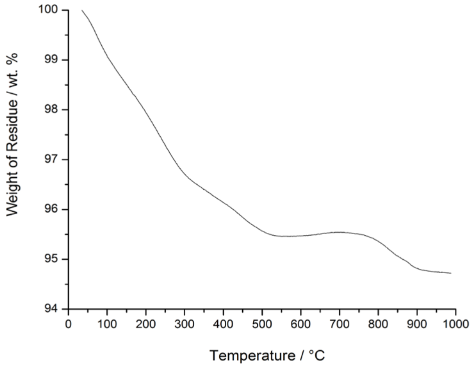

Fig. 5. TG curve for HAP/Gr coating.

2.4. Mechanical characteristics

Nanoindentation gives a key insight into mechanical properties of the materials, e.g. hardness and elastic modulus, thus offering a unique way of understanding of engineered materials on nanoscale level. Bone implants have to mimic characteristics of natural bone, in order to be successfully applied. However, exceptional brittleness of HAP, makes the HAP-based bone substitutes difficult to be handled during surgery and, therefore, there is a need for composite of HAP powders and HAP coatings with improved mechanical and adhesive properties. Hydroxyapatite coatings on metals are considered effective combination for hard tissue metallic implants, gaining maximum performance with minimum side-effects. The requirements for HAP-metal combination should exhibit a low elastic modulus, since the applied load is transferred to the healthy bone. Consequently, the coating-metal interface plays a significant role in providing the adequate mechanics.

The experimental values of mean hardness, H, mean reduced elastic modulus, E_r, and H/E ratio obtained from the nanoindentation testing of HAP, Ag/HAP, HAP/Gr and Ag/HAP/Gr coatings are presented in Table 2. The mean values and the standard deviation of hardness, H, obtained for the HAP/Gr and Ag/HAP/Gr coatings are 14.8 ± 2.0 GPa and 15.5 ± 3.3 GPa, respectively. Comparison between graphene-based coatings vs. their pure counterparts, HAP and Ag/HAP (7.4 ± 3.3 GPa and 14.5 ± 5.8 GPa) coatings the mean hardness is higher in the case of graphene-based coatings. Similarly, improvement in increasing of the mean reduced elastic modulus, E_r, of the HAP/Gr was 190.9 ± 18.0 GPa while E_r of Ag/HAP/Gr coatings 183.0 ± 21.9 GPa in comparison to HAP and Ag/HAP, 132.2 ± 25.5 GPa and 172.1 ± 36.9 GPa respectively [36, 46]. The impact of Ag addition is revealed by comparing Ag/HAP and pure HAP coating, as observed Ag contributed to the increase of both E_r (172.1 vs. 132.2 GPa) and H (14.5 vs. 7.40 GPa) [36, 46]. Addition of Gr as nanofiller even at this low concentration improves the mechanical properties of graphene-based coatings.

The ratio between H and E (H/E ratio) is called 'plasticity index' and it was first used as materials ranking parameter by Oberle [49], as a valuable measure in determining the limit of elastic behavior in a surface contact, which is clearly important to describes the 'elastic strain to failure'. The investigation of nanomechanical behavior of coatings revealed that H/E ratio values were 0.0774 for HAP/Gr and 0.0847 for Ag/HAP/Gr coatings, while in the case of their counterparts were 0.0560 for HAP and 0.0843 for Ag/HAP. This indicates that Gr reinforcement caused increase in the H/E ratio, implying that toughness values may be affected by Gr addition. Higher values of plasticity index indicate higher elastic properties and better adhesion to the substrate. Consequently, this can be attributed to the proposed toughening mechanism, i.e. grain-boundary toughening as a consequence of grain bridging by graphene nanosheets thus inhibiting crack propagation along the grain boundary. Based on the presented data, improved fracture toughness of the graphene-based composite coating is a result of crack bridging, deflection, and grain bridging by the Gr nanofiller.

Table 2

The values of mean hardness, H, mean reduced elastic modulus, E_r, and H/E ratio obtained from the nanoindentation testing of HAP, Ag/HAP, HAP/Gr and Ag/HAP/Gr coatings

Coating	H/GPa	E_r/GPa	H/E
HAP	7.4 ± 3.3	132.2 ± 25.5	0.0560
HAP/Gr	14.8 ± 2.0	190.9 ± 18.0	0.0774
Ag/HAP	14.5 ± 5.8	172.1 ± 36.9	0.0843
Ag/HAP/Gr	15.5 ± 3.3	183.0 ± 21.9	0.0847

2.5. Bioactivity

Bioactive HAP coating on Ti implants was able to stimulate the bone in growth and affixation to the implant surface during the early stage of implantation. The HAP shows excellent biocompatibility and osteoconductive properties. Even though apatite has an excellent biocompatibility, it has slow rate of osseointegration with bone tissues and hence, limits its applications. However, bioactive behaviour can be improved by incorporating a wide verity of anionic and cationic substitutions that exhibit an important role in the chemical, structural and microstructural properties [50].

The bioactivity of the HAP/Gr and Ag/HAP/Gr composite coatings was confirmed by the formation of an apatite layer after just 7 days soaking in SBF, as proven by FE-SEM analysis [36, 46]. The FE-SEM microphotograph in Fig. 6a and b displays the surface homogeneity of the HAP/Gr and Ag/HAP/Gr composite coating before immersion in SBF. Individual rod-like HAP grains, less than 50 nm in size, can be distinguished. In Fig. 6c and d, the FE-SEM image of the same HAP/Gr and Ag/HAP/Gr composite coatings after soaking in SBF, the newly formed apatite layer containing plate-shaped HAP crystals is clearly visible under high magnification (200,000×). The mineralization area ultimately penetrates the whole surface of the HAP/Gr composite. The morphology of the mineralization product varies dramatically with incorporation of Gr into the HAP matrix. Easily distinct are curled, plate-shaped apatite forms on the HAP/Gr composite coating. Also, the observed highly porous surface structure after soaking is beneficial for better cell adhesion, as it enables better connection between the implant and the bone. It has been reported [24] that open, interconnected porosity structures facilitate penetration of the surrounding bone tissue and hence lead to better biointegration and mechanical stability. Using XRD analysis [36, 46] the shift of characteristic HAP peaks at crystal planes (002), (211), and (300) toward higher angles is evident after immersing the HAP/Gr and Ag/HAP/Gr composite coating in

SBF for 7 days additionally confirmed the formation of new apatite layer, i.e. coatings bioactivity.

According to the mechanism proposed by Zhang et al. [3], the mineralization process proceeds in three stages: (1) dissolution controlled stage, (2) precipitation controlled stage, and (3) formation of bone-like apatite. In the first stage, dissolution of phosphate and calcium ions occurs. Calcium ion dissolution is governed by grain refinement and accelerates on the surface of the HAP/Gr coatings due to the suppression of HAP grain growth caused by adding Gr on the grain boundaries. As a result, the smaller grain size of the composite leads to increased specific area and improved interaction with SBF. In the second step, precipitation of an apatite layer occurs on the negative surface of the HAP/Gr coating as a consequence of the dissolution of calcium ions and subsequent emergence of nucleation sites. These events, elevated concentration of calcium ions in SBF, higher negative charge, and more available nucleation sites, allow the HAP/Gr composite coating to form a Ca-rich layer penetrating the whole sample surface. The third stage is the final formation of apatite as the Ca-rich layer attracts phosphate ions from the SBF and forms bonelike apatite clusters.

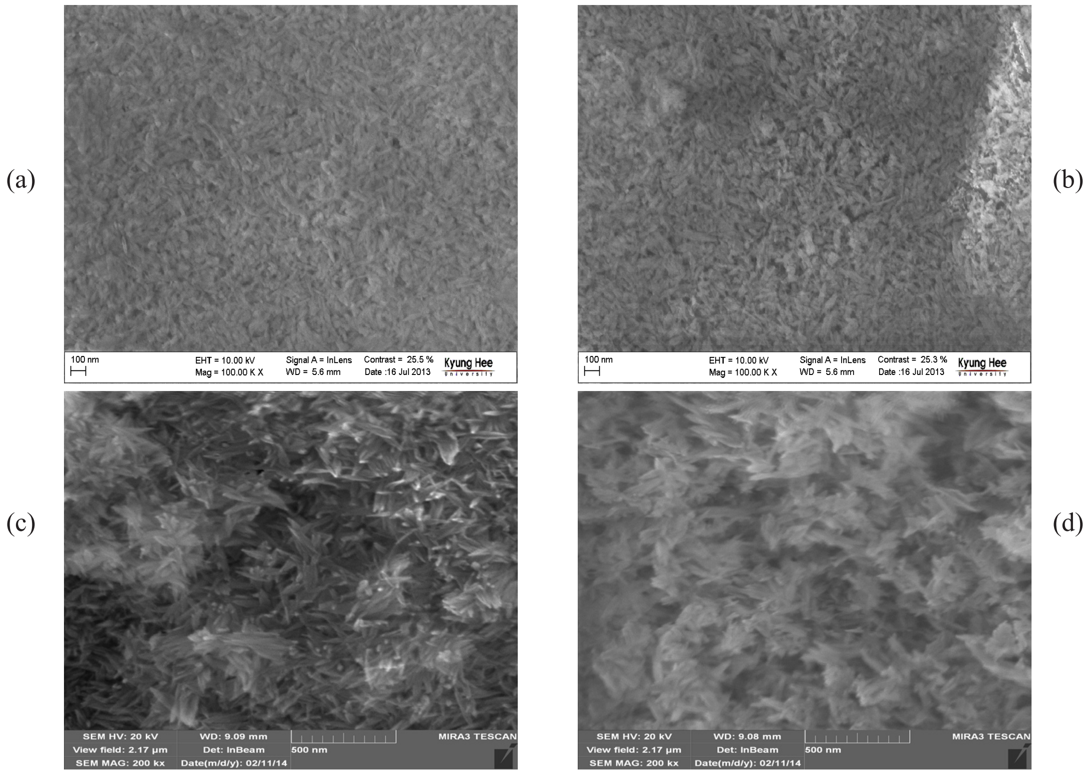

Fig. 6. FE-SEM microphotographs of the HAP/Gr and Ag/HAP/Gr coatings before (a, b) and after (c, d) 7 days immersion in SBF at 37 ºC.

2.6. Corrosion stability

Electrochemical impedance spectroscopy (EIS) as a sensitive and non-destructive method, had been used for the evaluation of the corrosion stability of the biocomposite HAP/Gr and Ag/HAP/Gr coatings in SBF solution and to predict bone implant behavior in the hostile environment such as human body. Fig. 7 shows Bode impedance spectra during different exposure times in SBF at 37 ºC for HAP/Gr and Ag/HAP/Gr coatings. The best fitting of EIS data was done by using the equivalent electrical circuits (EEC) (Fig. 8). EEC consist of the electrolyte resistance, R_s, the coating pore resistance, R_c, and CPE_c and CPE_{ox}, constant phase elements that represent all the frequency-dependent electrochemical phenomena, such as the coating capacitance, C_c, and passive oxide film capacitance, C_{ox}. CPE is used in these models to compensate for non-homogeneity in the system and is defined by two parameters, Y_0 and n. The impedance of CPE is represented by the following equation [51-53]:

$$Z_{\mathrm{CPE}} = \mathrm{Y}_{\mathrm{o}}^{-1} \cdot \left(\mathrm{j}\omega\right)^{-\mathrm{n}} \qquad (6)$$

where $j = (-1)^{1/2}$, $\omega = 2\pi f$ is the frequency in rad s^{-1}, and f is the frequency in Hz. If n values range from

0.8–1, the impedance of CPE can be considered to be the one of the pure capacitor:

$$Z_{\mathrm{CPE}} = \left(\mathrm{j}\omega C\right)^{-\mathrm{n}} \tag{7}$$

In this case Y_0 gives a pure capacitance (*C*). The impedance data in the complex plane were well fitted by the proposed EEC, and we used three basic criteria to evaluate the general accuracy of the fit: visual fit to Bode plots, low goodness of fit, and low relative standard errors for every circuit element [54]. We obtained suitably low goodness of fit ($<10^{-4}$), and the error associated with each element was lower than 10%. Thus, the chosen fit describes the investigated systems accurately. The obtained fitting values for each EEC parameter are presented in Table 3 for both graphene-based coatings. The n_c and n_{ox} values are higher than 0.80 for both graphene-based coatings, therefore $\mathrm{CPE_c}$ can be considered the coating capacitance, C_c, and $\mathrm{CPE_{ox}}$ can be considered the capacitance of the oxide film on the Ti surface beneath the coating, C_{ox}.

Table 3

EIS fitting results of EECs parameters for graphene-based coatings at various immersion times

t/h	R_s/Ω cm^2	R_c/kΩ cm^2	CPE$_c$/μFcm^{-2}	n_c	CPE$_{ox}$/μFcm^{-2}	n_{ox}	GOF
			Ag/HAP/Gr				
1	38.83	6.12	55.1	0.804	241	0.882	5.84e^{-4}
72	15.30	2.48	38.6	0.871	303	0.879	3.08e^{-5}
168	31.08	3.05	635.5	0.883	248	0.913	2.26e^{-5}
504	133.2	73.9	51.1	0.816	82	0.823	5.31e^{-4}
			HAP/Gr				
1	20.63	12.5	60.4	0.803	131	0.874	1.57e^{-4}
24	36.08	3.98	47.8	0.847	227	0.908	2.37e^{-5}
72	21.56	5.00	49.8	0.843	180	0.867	175e^{-4}
312	48.9	34.2	57.7	0.82	58	0.850	5.11e^{-4}

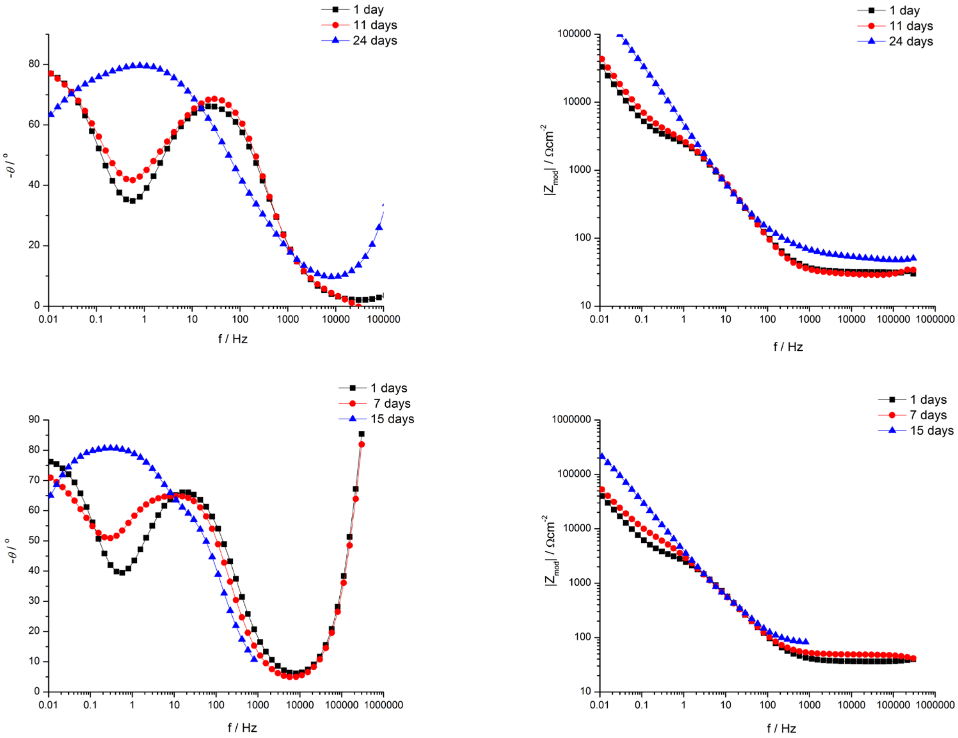

Fig. 7. Bode plots of Ag/HAP/Gr (a, b) and HAP/Gr (c, d) coatings after different immersion times in SBF solution at 37 ºC.

The Bode plots (Fig. 7a and b) for Ag/HAP/Gr coating appeared very similar shape upon increasing immersed time until 21 days and the EEC in Fig. 8a was used for fitting the EIS data. According to Table 2, R_c slightly decrease from 6.12 kΩ cm^2 during first hour to 2.48 kΩ cm^2 after 3 days, indicating that coating pores were filled with SBF. However, after 7 days R_c values started to increase, indicating the beginning of new apatite layer formation. Furthermore, after 21 days R_c achievied value of 73.9 kΩ cm^2 indicating the presence of newly formed carbonated HAP on coating surface. This suggests that the coating surface represented the site of nucleation and growth of new apatite layer. After 24 days the fitting of Bode modulus plot could only be done with the EEC in Fig. 8b that considers CPE$_{ox}$, indicating coating adhesion loss.

The phase shift plot showed two time constants in the case of the HAP/Gr composite coating during 14 days. The increase in phase angles at the low-frequency region may be associated with increasing values of R_c and beginning of the biomineralization process to form a new apatite layer onto the HAP/Gr surface. Finally, the calculated value of R_c was 34.2 kΩ cm^2 (Table 3) after 14 days of immersion in SBFsolution. The high value of the coating pore resistance denotes improved bioactivity, which suggests that the HAP/Gr coating surface represented a site of nucleation and growth for a new apatite layer recognized as carbonated HAP. However, the EEC in Fig. 8b was used for fitting the plot for the 15 days of SBF exposure, when coating adhesion loss had occurred.

The electrochemical studies suggested that both graphene-based coatings indicate a good corrosion resistance with an enhanced biomineralization and passivation of their surfaces.

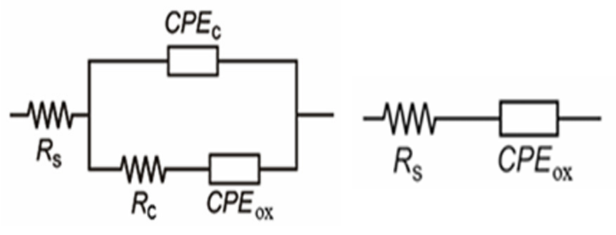

(a) (b)

Fig. 8. Equivalent electrical circuits used for fitting during prolonged immersion times in SBF solution.

2.7. Antibacterial activity and cytotoxicity

Infections of the implantation site are the major surgical problem worldwide. Serious complications that they cause often lead to revision surgeries. Therefore, we opted to test antibacterial activities of the samples against microorganisms responsible for the most of the inter-hospital infections, *Staphylococcus aureus* (Gram-positive bacterium) and *Escherichia coli* (Gram-negative bacterium). The results of qualitative antimicrobial agar diffusion tests showed that HAP/Gr did not inhibit either *Staphylococcus aureus* or *Escherichia coli* (data not shown), contrary to the Ag/HAP/Gr that affected both microorganisms (Fig. 9). The average inhibition zone was 2.5 mm for *Staphylococcus aureus* TL and it can be easily observed for the titanium plate in Fig. 9a. In the case of *Escherichia coli* (Fig. 9b), the average inhibition zone is much less pronounced, only 0.5 mm, barely distinguishable for titanium plate on the Petri dish.

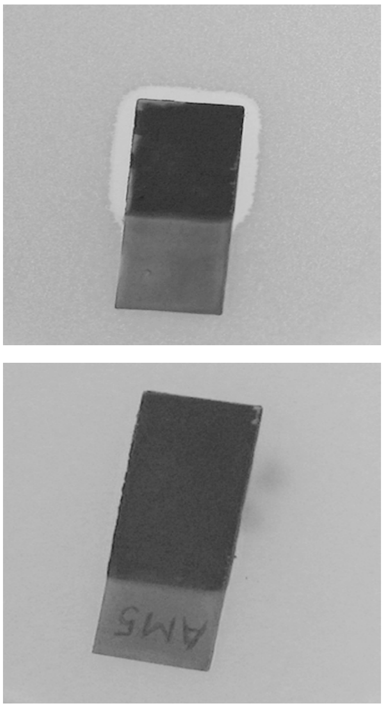

(a)

(b)

Fig. 9. Photographs of Ag/HAP/Gr samples against *Staphylococcus aureus* (a) and *Escherichia coli* (b).

Qualitative results were conclusive, but in order to verify and quantify the effect on *Staphylococcus aureus* that was more pronounced and therefore chosen microorganism for additional testing. The antibacterial properties of HAP/Gr and Ag/HAP/Gr samples were tested against the same strain of microorganisms liable for inter-hospital infections *Staphylococcus aureus* TL (Gram-positive bacterium) that we presumed our samples affected. Samples were investigated by monitoring changes in the viable number of bacterial cells in suspension (Fig. 10).

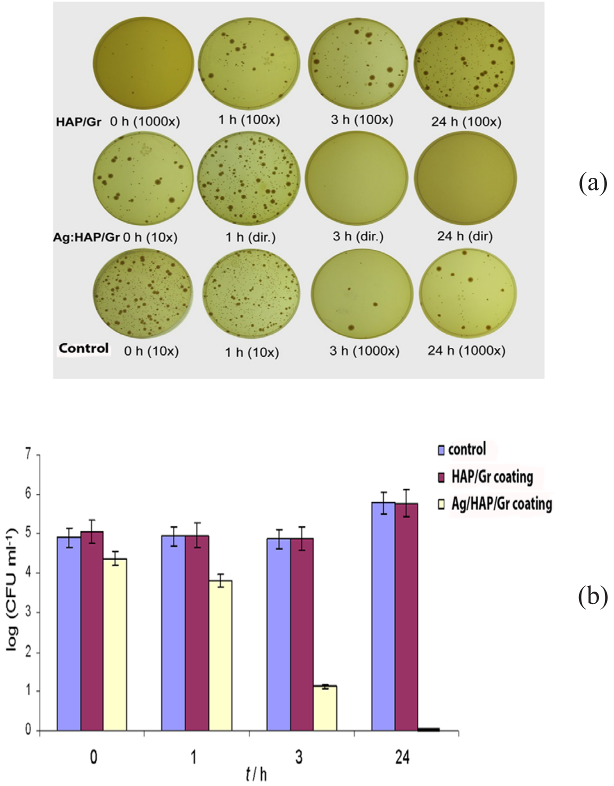

Fig. 10. Antibacterial activity of HAP/Gr and Ag/HAP/Gr coatings on LB agar plates, after 0, 1, 3 and 24 h; dilutions are denoted in parentheses (a) and reduction of viable cell number of *Staphylococcus aureus* TL after contact with HAP/Gr and Ag/HAP/Gr coatings for 0, 1, 3 and 24 h in PB as compared to the control w/o samples (b).

Figures 10a and 10b illustrate the antibacterial activity of Ag/HAP/Gr and HAP/Gr coatings against strains of *Staphylococcus aureus* TL. Figure 10a depicts the represented images of actual agar plates that were later enumerated, while Fig. 10b represents the data in the form of histogram. The antibacterial activity of Gr itself is controversial and demands further investigation. No antimicrobial activity of the HAP/Gr composite coating (Figs. 10a and b) could be noticed immediately after inoculation of samples. Cell viability did not change up to 3 h post incubation when compared to the initial number of cells in suspension. After 24 h of exposure noticeable bacterial growth was evident for both bacterial strains. Based on the presented data, HAP/Gr coatings exhibited no reduction of *Staphylococcus aureus* TL or *Escherichia coli* after 24 h, which is in agreement with previously conducted agar test. The same behavior of *Staphylococcus aureus* TL was reported in our previous work against a pure HAP coating [25]. However, these results further are inconclusive and do not help understand controversies regarding an antibacterial effect for Gr.

To the contrary to HAP/Gr samples, antimicrobial activity of the Ag/HAP/Gr coating (Figs. 9a and b) could be noticed immediately after inoculation of samples and further reduction of CFUs for two logarithmic units has been reached after just 1 h of incubation when compared to the initial number of cells in suspensions. Ag/HAP/Gr coating exhibited reduction of *Staphylococcus aureus* TL, since after 24 h, analyzed samples did not contain any visible colony even when samples were taken directly from the suspensions. Based on our results, an immediate silver ion release provides for the imminent drop in CFU numbers even after 1 h of exposure, which is in good agreement with bactericidal effect needed for prevention of biofilm formation [46].

The possibility of cytotoxic effect is another possible concern and therefore HAP/Gr and Ag/HAP/Gr coatings were submitted to a standard MTT test against PBMC cells. PBMC consist of lymphocytes and monocytes, thus representing one of the main populations of the human immune system cells [46]. For our initial testing, we investigated the coatings against PBMC as the first line of immune response against any type of implant in the human body, before proceeding to tissue specific cells (osteoblasts). *In vitro* cytotoxicity is usually evaluated by the MTT assay when screening biomaterials. The MTT assay is based on the reaction between MTT and mitochondrial succinate dehydrogenases in living cells to form a purple formazan soluble in dimethyl sulfoxide (DMSO) but insoluble in water. The optical density (OD) value of formazan–DMSO solution is considered to be proportional to the number of living cells. Mandatory requirement for biomaterials is that they exert no toxic effects against the surrounding tissue. Cell survival of PBMCs, calculated for HAP/Gr was 72.3 ± 4.3% [36]. PBMCs in the presence of Ag/HAP/Gr coating displayed 79.6 ± 11.2% survival [46]. Overall, both graphene-based composite coatings showed a mild decrease in the survival of healthy immunocompetent PBMC compared to the control cell sample, with Ag/HAP/Gr coating as the possible bactericidal composite also is best non-cytotoxic candidate.

3. Conclusions

The presented EPD method proved to be a convenient technique of successfully obtaining novel graphene based biocomposites Ag/HAP/Gr and HAP/Gr coatings on a Ti foil. Rod like grain structure of hydroxyapatite was visualized in FE-SEM images of the Ag/HAP/Gr and HAP/Gr coating surfaces that also revealed less cracks for the graphene based coatings than for their pure counterparts. According to XPS analysis, the calculated Ca/P ratio of 1.58 for the HAP/Gr and 1.52 for the Ag/HAP/Gr are greater than the Ca/P ratio for the pure HAP and Ag/HAP coating of 1.50 and closer to the stoichiometric value. The greater thermal stability of Ag/HAP/Gr and HAP/Gr coating compared to the Ag/HAP and HAP coating was confirmed by TGA, emphasizing improvements brought in by graphene addition. The nanoindentation results are a definite demonstration that introducing graphene nanosheets improved the mechanical properties of both Ag/HAP and HAP powders effectively. XRD, FE-SEM and EIS analyses clearly confirm the bioactivity of the HAP/Gr and Ag/HAP/Gr coatings in the formation of an apatite layer after soaking in SBF. No antibacterial effect of HAP/Gr coating could be observed against bacteria *Staphylococcus aureus* TL and *Escherichia coli*, based on tests in suspension results and agar diffusion tests. On the other hand, Ag/HAP/Gr coating exhibited strong antibacterial activity against *Staphylococcus aureus* after only 3 h of exposure, therefore suppressing harmful biofilm formation. The HAP/Gr and Ag/HAP/Gr coatings were classified as non-cytotoxic within the margin of error against the targeted PBMC.

Therefore, the evidence presented here demonstrates that a nanosized graphene-based coatings produced by EPD are excellent candidates for future biomedical Ti implants.

Acknowledgements

This work was supported by a grant from Kyung Hee University in 2012 (KHU-20130359) and the Basic Science Research Program through the National Research Foundation of Korea (NRF) funded by the Ministry of Education, Science and Technology (2011-0013066). This research was also financed by the Ministry of Education, Science and Technological Development, Republic of Serbia, contract No. III 45019.

The authors would like to thank Dr. Maja Vukašinović-Sekulić, Faculty of Technology and Metallurgy, University of Belgrade, for performing antibacterial testing and analysis and for helpful discussions and also to Dr. Veljko Djokic, Faculty of Technology and Metallurgy, University of Belgrade, for his help in the FE-SEM analysis.

References

[1]. G.M. Neelgund, A. Oki, and Z. Luo, Mater. Res. Bull. 48 (2013) 175–179.
[2]. A.R. Biris, S. Ardelean, M.D. Lazar, E. Dervishi, F. Watanabe, A. Ghosh, A. Biswas, and A.S. Biris, Carbon 50 (2012) 2252–2263.
[3]. L. Zhang, W. Liu, C. Yue, T. Zhang, P. Li, Z. Xing, and Y. Chen, Carbon 61 (2013) 105–115.
[4]. J. Liu, H. Yan, M.J. Reece, and K. Jiang, J. Eur. Ceram. Soc. 32 (2012) 4185–4193.
[5]. T. Kuilla, S. Bhadra, D. Yao, N.H. Kim, S. Bose, and J.H. Lee, Prog. Polym. Sci. 35 (2010) 1350–1375.
[6]. S.F. Bartolucci, J. Paras, M.A. Rafiee, J. Rafiee, S. Lee, D. Kapoor, and N. Koratkar, Mater. Sci. Eng. A 528 (2011) 7933–7937.
[7]. M. Belmonte, C. Ramírez, J. González-Julián, J. Schneider, P. Miranzo, and M.I. Osendi, Carbon 61 (2013) 431–435.
[8]. Y. Liu, Z. Dang, Y. Wang, J. Huang, and H. Li, Carbon 67 (2014) 250–259.
[9]. G. Manivasagam, D. Dhinasekaran, and A. Rajamanickam, Recent Pat. Corros. Sci. 2 (2010) 40–54.
[10]. S. Baradaran, E. Moghaddam, W.J. Basirun, M. Mehrali, M. Sookhakian, M. Hamdi, M.R. Nakhaei Moghaddam, and Y. Alias, Carbon 69 (2014) 32–45.
[11]. M. Li, Y. Wang, Q. Liu, Q. Li, Y. Cheng, Y. Zheng, T. Xi, and S. Wei, J. Mater. Chem. B 1 (2013) 475–484.
[12]. L.M. Rodriguez-Lorenzo, L. Benito- Garzón, F. Barroso-Bujans, and M. Fernández, Key Eng. Mater. 477 (2008) 396–398.
[13]. J. Zhu, H.M. Wong, K.W.K. Yeung, and S.C. Tjong, Adv. Eng. Mater. 13 (2011) 336–341.
[14]. S. Kim, S.H. Ku, S.Y. Lim, J.H. Kim, and C.B. Park, Adv. Mater. 23 (2011) 2009–2014.
[15]. H. Liu, P. Xi, G. Xie, Y. Shi, F. Hou, L. Huang, F. Chen, Z. Zeng, C. Shao, and J. Wang, J. Phys. Chem. C 116 (2012) 3334–3341.
[16]. A.R. Biris, M. Mahmood, M. Lazar, E. Dervishi, F. Watanabe, T. Mustafa, G. Baciut, M. Baciut, S. Bran, S. Ali, and A.S. Biris, J. Phys. Chem. C 115 (2011) 18967–18976.
[17]. H.B. Ma, W.X. Su, Z.X. Tai, D.F. Sun, X.B. Yan, B. Liu, and Q.J. Xue, Chinese Sci. Bull. 57 (2012) 3051–3058.
[18]. M.A. Rafiee, J. Rafiee, I. Srivastava, Z. Wang, H.H. Song, Z.Z. Yu, and N. Koratkar, Small 6 (2) (2010) 179–183.
[19]. D. Lahiri, S. Ghosh, and A. Agarwal, Mater. Sci. Eng. C, 32 (7) (2012) 1727–1758.
[20]. S. Park, and R.S. Ruoff, Nat. Nanotechnol. 4 (4) (2009) 217–224.
[21]. M. Kalbacova, A. Broz, J. Kong, and M. Kalbac, Carbon 48 (15) (2010) 4323–4329.
[22]. W.B. Hu, C. Peng, W.J. Luo, M. Lv, X.M. Li, D. Li, Q. Huang, C. Fan, ACS Nano 4 (7) (2010) 4317–4323.

[23]. H.Y. Liu, P.X. Xi, G.Q. Xie, Y.J. Shi, F.P. Hou, L. Huang, F. Chen, Z. Zeng, C. Shao, and J. Wang, J. Phys. Chem. C 116 (5) (2012) 3334–3341.

[24]. S. Eraković, A. Janković, Dj. Veljović, E. Palcevskis, M. Mitrić, T. Stevanović, Dj. Janaćković, and V. Mišković-Stanković, J. Phys. Chem. B 117 (6) (2013) 1633–1643.

[25]. S. Erakovic, A. Jankovic, I. Z. Matić, Z.D. Juranić, M. Vukašinović-Sekulić, T. Stevanović, and V. Mišković-Stanković, Mater. Chem. Phys. 142 (2013) 521–530.

[26]. A.R. Boccaccini, S. Keim, R. Ma, Y. Li, and I. Zhitomirsky, J. R. Soc. Interface 7 (2010) S581–S613.

[27]. I. Corni, M.P. Ryan, and A.R. Boccaccini, J. Eur. Ceram. Soc. 28 (7) (2008) 1353–1367.

[28]. A.R. Boccaccini, J. Cho, T. Subhani, C. Kaya, and F. Kaya, J. Eur. Ceram. Soc. 30 (5) (2010) 1115–1129.

[29]. C. Kaya, I. Singh, and A.R. Boccaccini, Adv. Eng. Mater. 10 (1-2) (2008) 131–138.

[30]. Y.W. Song, D.Y. Shan, and E.H. Han, Mater. Lett. 62 (17-18) (2008) 3276–3279.

[31]. M.S. Djošić, Z.M. Kačarević-Popović, B.M. Jokić, N. Bibić, M. Mitrić, S.K. Milonjić, R. Jančić-Heinemann, and J. Stojanović, Colloid Surf. A 341(1-3) (2009) 110–117.

[32]. V.B. Misković-Stanković, Electrophoretic Deposition of Ceramic Coatings on Metal Surfaces. In: Stojan S. Djokić, editor. Electrodeposition and Surface Finishing: Fundamentals and Applications, Modern Aspects of Electrochemistry, vol 57, New York; Springer Science+Business Media; 2014, p. 133–216.

[33]. P. Sarkar, and P.S. Nicholson, J. Am. Ceram. Soc. 79(8) (1996) 1987–2002.

[34]. S. Eraković, Dj. Veljović, P.N. Diouf, T. Stevanović, M. Mitrić, Dj. Janaćković, I.Z. Matić, Z.D. Juranić, and V. Mišković-Stanković, Prog. Org. Coat. 75(4) (2012) 275–283.

[35]. S. Eraković, Dj. Veljović, P.N. Diouf, T. Stevanović, M. Mitrić, S. Milonjić, and V. Mišković-Stanković, Int. J. Chem. React. Eng. 7:A62 (2009).

[36]. A. Janković, S. Eraković, M. Mitrić, I.Z. Matić, Z.D. Juranić, G.C.P. Tsui, C.-Y. Tang, V. Mišković-Stanković, K.Y. Rhee, and S.J. Park, J. All. Comp. 624 (2015)148–157.

[37]. K.N. Kudin, B. Ozbas, H.C. Schniepp, R.K. Prudhomme, I.A. Aksay, and R. Car, Nano Lett. 8 (1) (2008) 36–41.

[38]. S. Erakovic, A. Jankovic, C. Ristoscu, L. Duta, N. Serban, A. Visan, I.N. Mihailescu, G.E. Stan, M. Socol, O. Iordache, I. Dumitrescu, C.R. Luculescu, Dj. Janackovic, and V. Miskovic-Stankovic, Appl. Surf. Sci. 293 (2014) 37–45.

[39]. C.-C. Wu, S.-T. Huang, T.-W. Tseng, Q.-L. Rao, and H.-C. Lin, J. Mol. Struct. 979 (2010) 72–76.

[40]. Z. Fan, J. Wang, Z. Wang, H. Ran, Y. Li, L. Niu, P. Gong, B. Liu, S. Yang, Carbon 66 (2014) 407–416.

[41]. P. Lian, X. Zhu, S. Liang, Z. Li, W. Yang, and H. Wang, Electrochim. Acta 55 (12) (2010) 3909–3914.

[42]. E.C. Victoria, and F.D. Gnanam, Trends Biomater. Artif. Organs 16(1) (2002) 12–14.

[43]. A. Roguska, M. Pisarek, M. Andrzejczuk, M. Dolata, M. Lewandowska, and M. Janik-Czachor, Mater. Sci. Eng. C 31(5) (2011) 906–914.

[44]. Z.Q. Yao, Yu. Ivanisenko, T. Diemant, A. Caron, A. Chuvilin, J.Z. Jiang, R.Z. Valiev, M. Qi, and H.-J. Fecht, Acta Biomater. 6 (7) (2010) 2816–2825.

[45]. K.M. Watling, J.F. Parr, L. Rintoul, C.L. Brown, and L.A. Sullivan, Spectrochim. Acta A 80 (1) (2011) 106–111.

[46]. V. Mišković-Stanković, A. Janković, S. Eraković, K.Y. Rhee, VIII International Symposium Physics and Chemistry of Carbon Materials/ Nanoengineering, Almaty, The Republic of Kazakhstan, 2014, Proceedings, p. 21–23.

[47]. M. Li, Q. Liu, Z. Jia, X. Xu, Y. Shi, Y. Cheng, Y.F. Zheng, T.F. Xi, S.C. Wei, Carbon 67 (2013)185–197.

[48]. V.H. Nguyen, B.K. Kim, Y.-L. Jo, and J.-J. Shim, J. Supercrit. Fluids 72 (2012) 28–35.

[49]. A. Leyland, and A. Matthews, Wear 246 (2000) 1–11.

[50]. S. Sutha, K. Kavitha, G. Karunakaran, V. Rajendran, Mater. Sci. Eng. C, 33 (2013) 4046–4054.

[51]. M.M. Popović, B.N. Grgur, and V.B. Mišković–Stanković, Prog. Org. Coat. 52(4) (2005) 359–365.

[52]. M. Sluyters-Rehbach, Pure, Appl. Chem. 66 (9) (1994) 1831–1891.

[53]. V.D. Jović, and B.M. Jović, J. Electroanal. Chem. 541 (2003) 1–11.

[54]. M.E. Orazem, and B. Tribollet, Electrochemical impedance spectroscopy. Hoboken: New Jersey: John Wiley & Sons, Inc; 2008.

Received 10 September 2014